Journal of Neuroscience Methods 388 (2023) 109810

Contents lists available at ScienceDirect

Journal of Neuroscience Methods

journal homepage: www.elsevier.com/locate/jneumeth

# Controlling jaw-related motion artifacts in functional near-infrared spectroscopy

Fan Zhang [a], Adaira Reid [a], Alissa Schroeder [a], Lei Ding [a,b], Han Yuan [a,b,*]

[a] Stephenson School of Biomedical Engineering, University of Oklahoma, Norman, OK 73019, USA
[b] Institute for Biomedical Engineering, Science and Technology, University of Oklahoma, Norman, OK 73019, USA

ARTICLE INFO

*Keywords:*
Functional near-infrared spectroscopy
Motion artifacts
Jaw
Temporalis muscle
Auditory response
Resting-state functional connectivity

ABSTRACT

*Background:* Functional near-infrared spectroscopy (fNIRS) as a non-invasive optical neuroimaging technique has demonstrated great potential in monitoring cerebral activity. Due to its portability and compatibility with medical implants, fNIRS has seen increasing applications in studying the hearing, language and cognitive functions. However, fNIRS is susceptible to artifacts related to jaw movements, such as teeth clenching, swallowing and speaking, which affect recordings over the temporal, parietal and frontal/prefrontal cortices.
*New method:* We investigated two new approaches to control the jaw-related motion artifacts, an individually customized bite bar apparatus and a denoising algorithm namely PCA-GLM based on multi-channel fNIRS recordings from long-separation and short-separation montage. We first recorded data while subjects performed a clenching task, then an auditory task and a resting-state task with and without the bite bar.
*Results:* Our results have shown that jaw clenching can introduce spurious, task-evoked-like responses in fNIRS signals. A bite bar customized for each participant effectively suppressed the movement-related activities in fNIRS, at both task and resting-state conditions. Moreover, the bite bar and the PCA-GLM denoising method are shown to improve auditory responses, by significantly reducing the within-subject standard deviation, increasing the task-related contrast-to-noise ratio, and yielding stronger activations to the auditory stimuli.
*Comparison with existing method(s):* The current study has demonstrated a novel method to control the jaw-related motion artifacts in fNIRS signals.
*Conclusions:* Our method will benefit the study of the hearing, language and cognitive functions in normal healthy subjects and patients.

## 1. Introduction

Functional near-infrared spectroscopy (fNIRS) is a noninvasive neuroimaging technology that measures hemodynamic responses in the human brain using near-infrared light (Scholkmann et al., 2014). Compared to functional magnetic resonance imaging (fMRI), it provides the advantage of affordable cost, portability, low operating noise, and compatibility with electronic or magnetic stimulation devices, such as cochlear implants (Chiarelli et al., 2017; Luke et al., 2021; Scholkmann et al., 2014). Recently, fNIRS has drawn increasing interest in studying the hearing, language, and other cognitive functions in the human brain (Pollonini et al., 2014; Saliba et al., 2016). For example, fNIRS can be used in infants who have cochlear implants and are unable to verbally communicate their hearing and comfort when adjusting sound levels (Bortfeld, 2019). The understanding of auditory perception mechanisms of normal sound and cochlear stimuli can facilitate the early intervention of hearing loss in infants to preserve and develop their speech and language function. Another exemplary work is to use wearable fNIRS to assess and monitor the cognitive decline in elderly individuals with mild cognitive impairment (Maidan et al., 2016; Makizako et al., 2013). Furthermore, fNIRS as a broadly accessible tool that can image the brain-wide resting state functional connectivity offers advantages in studying aging populations (Khan et al., 2022, 2021; Zhang et al., 2022a).

However, there are critical confounding factors in fNIRS signals, including interferences from superficial layers of the head, systemic physiological noises and motion artifacts (von Lühmann et al., 2019, 2020; Zhang et al., 2021). Although less vulnerable to head movements, fNIRS can still be affected by jaw movements during teeth clenching, speaking and swallowing, which involves contractions of the temporalis

* Correspondence to: 173 Felgar Street, Gallogly Hall, Room 101, Norman, OK 73019, USA.
*E-mail address:* hanyuan@ou.edu (H. Yuan).

https://doi.org/10.1016/j.jneumeth.2023.109810
Received 30 August 2022; Received in revised form 29 December 2022; Accepted 30 January 2023
Available online 2 February 2023

muscles (Novi et al., 2020; Schecklmann et al., 2017). The jaw movements could result in blood flow changes in the temporalis muscle as well as displacement between the optodes and the scalp, leading to artifacts in the fNIRS signals (Schecklmann et al., 2017). While many previous studies have investigated head movements (Cui et al., 2010; Fishburn et al., 2019; Izzetoglu et al., 2010; Scholkmann et al., 2010), the impact and handling of jaw movements remain largely unclear (Novi et al., 2020; Schecklmann et al., 2017).

In our pilot work, we have studied the motion artifacts related to several types of jaw movements, including clenching, speaking, swallowing and sniffing, and reported that jaw movements produced prominent and robust artifacts in fNIRS signals (Zhang et al., 2022b). In this study, we aimed to address the issue of jaw-related motion artifacts in fNIRS, by testing whether an individually customized bite bar can control jaw movements, and furthermore evaluating whether our previously established denoising pipeline namely PCA-GLM (Zhang et al., 2021) can correct the motion artifacts in fNIRS signals. We acquired experimental data in healthy subjects performing three tasks – a jaw clenching task, an auditory task and a resting-state task. Before each experiment, we customized a bite bar for each participant. The auditory and resting-state recordings were acquired repeatedly with and without using a bite bar. Data were processed with a minimal preprocessing pipeline and our previously established PCA-GLM denoising method (Zhang et al., 2021). Quantitative metrics evaluated the amount of motion and the effects of the bite bar and the denoising algorithm in improving auditory response. We also investigated the resting state functional connectivity.

## 2. Material and methods

### 2.1. Participants

All study protocols were approved by the Institutional Review Boards at The University of Oklahoma Health Sciences Center. A total of ten healthy subjects without acute jaw and teeth problems participated in this study. Informed consent was obtained from study participants. Data from one participant were excluded due to bad coupling between optodes and scalp. Therefore, data from nine participants (six females, 23.1 ± 5.9 years old) were used for the analyses. Participants received financial compensation for their participation.

### 2.2. Design of bite bar

Bite bars were made using a plastic piece and vinyl polysiloxane putty for each subject. Specifically, a plastic piece was first created using Adobe Illustrator (Adobe Systems Inc., San Jose, CA, USA). This piece was then laser cut out of quarter-inch-thick acrylic at the University of Oklahoma Fabrication Lab. The piece measured 4 × 1.5 in. with a 1.25-inch diameter semicircular cutout on the narrower end. The bite bar was assembled by combing the plastic piece and dental putty. The putty used here was vinyl polysiloxane, which was made by mixing 5 mL putty base and 5 mL putty catalyst thoroughly for 1 min. The mixture putty was then formed around a bite piece and placed in the subject's mouth such that the bite bar was inserted comfortably approximately 1–2 in. deep. The subject was then instructed to bite down firmly while the putty was molded by their teeth for three minutes. After the putty was molded, the bite bar was ready for use in the experiment. A picture of the bite bar customized for one of the subjects is shown in Fig. 1.

(A) A customized bite bar. The bite bar was assembled using dental putty (top) and a plastic piece (bottom). (B) Arrangement of fNIRS

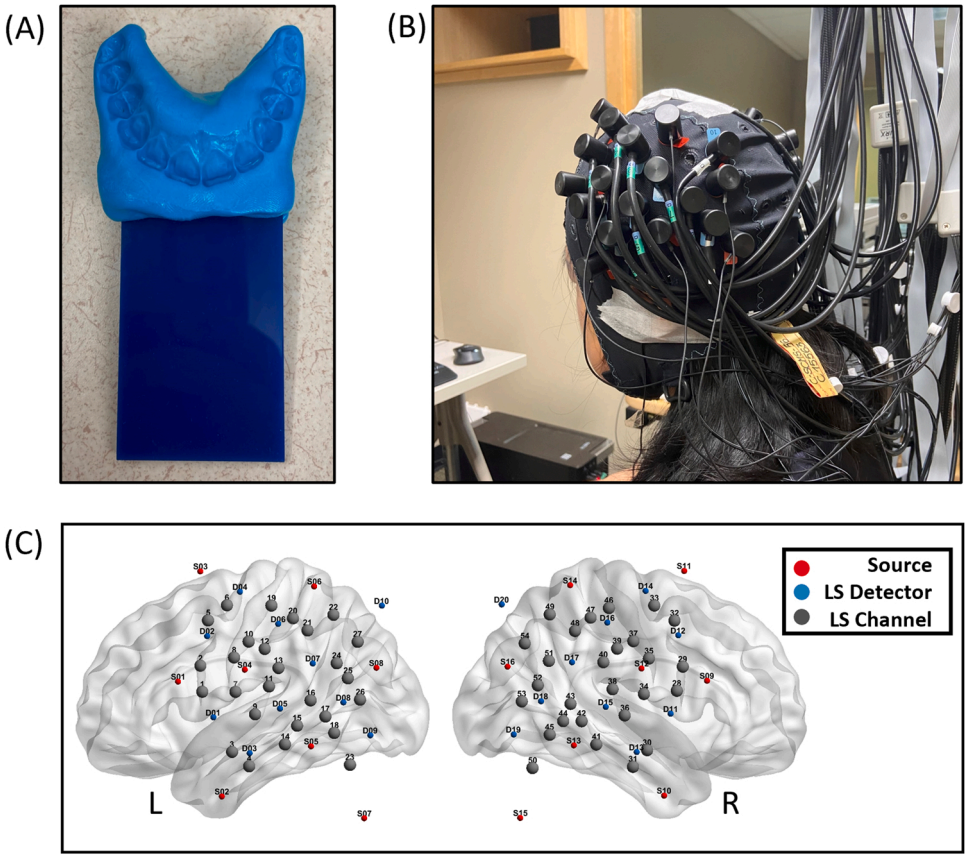


**Fig. 1.** Experimental settings.

optodes in a participant. (C) Illustration of the fNIRS optodes covering the auditory and parietal cortices. The red solid circles, blue solid circles, and gray solid circles indicate fNIRS sources, long-separation (LS) detectors and LS channels, respectively.

### 2.3. Experimental paradigm

Participants were instructed to perform three types of tasks in a comfortable sitting position with their eyes open. Specifically, each participant performed (1) two sessions of jaw-clenching task, (2) three sessions of auditory task without biting a bite bar, (3) three sessions of auditory task while biting a bite bar, (4) two sessions of resting-state task without biting a bite bar and (5) two sessions of resting-state task while biting a bite bar. The order of with-bite-bar vs. without-bite-bar conditions was counterbalanced in two sequences, to which participants were randomly assigned. A jaw-clenching session consisted of seven blocks, each of which included a 20-s clenching period and a 30-s resting period. During the clenching period, the participants were instructed to perform the jaw clenching three times at 0.15 Hz (i.e., with an interval of 6.67 s) guided by a visual cue. An auditory session consisted of seven blocks, each including an auditory stimuli period of 20 s and a resting period of 30 s. The auditory stimulus was adapted from a previous study (Chen et al., 2015) and consisted of two pure tones of 554 and 440 Hz. The tones were sampled at 44.1 kHz and were alternated, starting with the 554 Hz tone. Each tone lasted 500 ms with a 50-ms linear rise and fall. The stimulus was made in the Adobe Audition software (Adobe Systems Inc., San Jose, CA, USA). Each resting session lasted six minutes. In total, 10 sessions of recording were acquired from each subject. E-Prime (Psychology Software Tools, Sharpsburg, PA) software was used to display instructions and present the tasks on an LCD monitor. The auditory stimuli were played at a calibrated, fixed sound volume (70 dB) through two earbuds worn in the ears of participants.

### 2.4. Data acquisition

A NIRScout system (NIRX, New York, United States) was used to collect fNIRS data at a sampling rate of 3.91 Hz. A total of 16 light sources (760 nm and 850 nm) and 20 light detectors were arranged over the left and right auditory cortices to form an array with 54 long-separation (LS) channels at about 30-mm distance. In addition, 16 short-separation (SS) (8-mm) detectors were placed around each source and constructed 16 SS channels. Figs. 1B and 1C show the instrument setting and the layout of fNIRS optodes, respectively. The cortical visualizations were generated with BrainNet Viewer (Xia et al., 2013) and NIRS-KIT (Hou et al., 2021), based on the standard coordinates of fNIRS sources and detectors. Physiological measurements including triaxial acceleration, respiration, and cardiac pulsation were also simultaneously collected by a 64-channel actiCHamp system (Brain Vision, North Carolina, United States), following the protocol described in Zhang et al. (2021).

### 2.5. fNIRS data preprocessing

fNIRS data were preprocessed using Homer2 (Huppert et al., 2009) and proprietary codes in MATLAB® (The Mathworks, Natick, MA) reported in our previous work (Zhang et al., 2021). Specifically, the steps are: (1) converting the raw data into optical densities (OD); (2) calculating the power spectral densities of each channel using the Welch's method with window length of 60 s and 50 % overlap, and rejecting bad channels which showed no peak at heartbeat frequency range (0.8–1.6 Hz); (3) bandpass filtering OD with 0.008–0.2 Hz; (4) converting the filtered OD to relative changes of oxy-hemoglobin (HbO) and deoxy-hemoglobin (HbR) using the modified Beer-Lambert law (MBLL) (Scholkmann et al., 2014). The differential pathlength factors of 7.25 and 6.38 were used for 760 nm and 850 nm, respectively (Herold et al., 2018). The molar extinction coefficients were 645.5 $cm^{-1}$/M and 1097.0 $cm^{-1}$/M for HbO and 1669.0 $cm^{-1}$/M and 781.0 $cm^{-1}$/M for HbR at 760 nm and 850 nm, respectively (Piper et al., 2014).

### 2.6. Denoising fNIRS signals with PCA-GLM method

A general linear model (GLM) was configured per session for measuring the task effect. A third-order polynomial drift and a hemodynamic response function (HRF) regressor which accounts for the task were included in the design matrix. The HRF regressor was derived by convolving the boxcar of stimuli with a canonical two-gamma HRF model (Lindquist et al., 2009). This GLM model based on minimal preprocessed data was referred to as No Correction.

Furthermore, the PCA-GLM denoising method (Zhang et al., 2021) was applied to remove jaw-related artifacts. A more comprehensive regression model was configurated per session according to the published procedure. Specifically, principal component analysis (PCA) was first applied to multi-channel LS and SS data separately. A noise component of the LS data designated as PC-LS was automatically identified by the highest value of the coefficient of spatial uniformity (CSU) (Kohno et al., 2007). Then, the time course of PC-LS was used to automatically identify a component of the SS data by the highest temporal correlation with PC-LS, designated as PC-SS. The PC-SS was then included as a nuisance regressor in the GLM to be removed. Additionally, the auxiliary measurements of triaxial acceleration, respiration and pulsation were bandpass filtered with 0.008–0.2 Hz, detrended by a third-order polynomial drift and then utilized as nuisance regressors. Like the processing of No Correction, a third-order polynomial drift and a task-related HRF regressor were included in the design matrix.

### 2.7. Block averages and topographies

For clenching and auditory tasks, the block averages were calculated by removing the baseline (i.e., mean amplitude of −5 to 0 s to the onset of each block) and calculating the mean across seven blocks. Standard errors were calculated in the block averaging process.

To visualize the tasked-evoked activations to auditory stimuli, we calculated the topographies based on block averages of HbO. The averaged HbO amplitude during a stimulation window (5–18 s) was compared to the averaged HbO amplitude during a resting window (20–30 s) by a two-tailed paired-sample t-test, following a more sensitive approach of detecting the fNIRS activations (Wu et al., 2022). Multiple comparisons correction on the topographies was addressed by the Benjamini-Hochberg procedure, resulting in a false discovery rate ($q$) thresholded at 0.05 (Benjamini and Hochberg, 1995).

Channels of interest were identified – namely the clenching channel and the auditory channel. Based on the group-level HbO topography of the clenching condition, channels with the most prominent motion artifacts were noted and designated as the clenching channels (one on the left hemisphere and the other on the right hemisphere). Meanwhile, for the auditory channel, an fNIRS channel of representative responses to the stimuli, was selected based on the group-level HbO topography.

### 2.8. Characterization of motion artifacts

To assess the effects of jaw clenching on fNIRS signals and the efficacy of bite bar in suppressing jaw-related motion artifacts, we utilized a motion detection metric termed global variance of temporal derivatives (GVTD) which has been shown to strongly correlate with auxiliary measures of motion (Sherafati et al., 2020). Specifically, we calculated GVTD according to the following equation:

$$g = \begin{bmatrix} g_1 \\ \vdots \\ g_M \end{bmatrix}, g_i = \sqrt{\frac{1}{N}\sum_{j=1}^{N}\left(y_{ji} - y_{ji-1}\right)^2}$$

where $i$ indexes the time point, $j$ indexes the fNIRS channel, g is the

GVTD vector (thus a time course), $y_{ji} \in \mathbb{R}$is the optical densities after bandpass filtering of 0.008–0.2 Hz at the $j$-th channel. The optical densities of both wavelengths were pooled together for the calculation of GVTD. The resulting GVTD time course represents the global co-fluctuation across all channels regardless of the sign/direction of the fluctuations. To assess whether jaw clenching introduces motion artifacts in fNIRS signals, the means of GTVD in the clenching period (0–20 s in each block) and the resting period (20–50 s in each block) were calculated for each session. A two-tailed paired-sample t-test was performed to determine whether there are significant differences in GVTD between the clenching and resting periods. In addition, to visualize the GVTD metric at instructed motion periods, the group-level GVTD time course was obtained by averaging the GVTD time courses from all sessions.

To assess whether a bite bar is effective in suppressing jaw-clenching movements, the mean GVTD across each session was calculated for auditory and resting-state tasks. A two-tailed paired-sample t-test was performed to determine whether any significant differences in mean GVTD between auditory/resting data without and with an individually customized bite bar addressed to each subject.

### 2.9. Evaluation of motion control performance in auditory task

In addition to quantify the amount of motion as described above, our study chose an experimental task to examine in more details how the motion control would benefit, or what the impact would look like, in the context of a typical fNIRS research task. A systematic evaluation was performed on the auditory experimental data, because the ground truth is expected in such a well-established task that task-related increases in HbO should be *present* in auditory channels whereas in non-auditory channels, task-related changes in HbO should be *absent*. We chose the auditory task rather than the clenching task for evaluation, because we wanted the evaluation to be meaningful in a realistic experiment condition, although our preliminary findings in a prior publication (Zhang et al., 2022b) have already shown that PCA-GLM can suppress the jaw-related activities in a voluntary clenching task.

A total of four evaluation metrics were calculated, including within-subject standard deviation (SD), contrast-to-noise ratio (CNR), mean amplitudes and beta values of the HRF regressor, following our previous denoising study (Zhang et al., 2021).

(1) The within-subject SD (Brigadoi et al., 2014) is calculated as the standard deviation across blocks of a single session when calculating the block averages.
(2) CNR is calculated as the difference between the mean amplitudes during the task and the rest period normalized by the summation of variances at task and rest periods (Cui et al., 2010; Nguyen et al., 2018; Zhang et al., 2005). The CNR is defined as follows:

$$CNR = \frac{mean(task) - mean(rest)}{\sqrt{\mathrm{var}(task) + \mathrm{var}(rest)}} \quad (1)$$

where "task" denotes the task period (from 6 s to 18 s), and "rest" denotes the resting period (from −5 s to 0 s) with respect to the onset of each task block (t = 0 s). A high CNR value indicated that the ratio of task-evoked signal to noise is high.
(3) The mean amplitude is defined as the averaged amplitude of the relative concentration changes during a window (5–18 s) within the stimuli period (Strangman et al., 2002).
(4) The beta value of the task-related HRF regressor is produced by the GLM regression, with positive values indicating task-related increase and negative values indicating task-related decrease.

In statistical analysis, a two-way analysis of variance (ANOVA) with the bite bar and the denoising method as factors was performed on each of the four quantitative metrics (beta value, CNR, mean amplitude and within-subject SD) of the LS channel. The two-way ANOVA was constructed on metric data corresponding to four different combinations including [No Bite Bar, No Correction], [Bite Bar, No Correction], [No Bite Bar, PCA-GLM] and [Bite Bar, PCA-GLM].

To visualize the effect by the bite bar and PCA-GLM, topographies of differences are plotted, respectively. The topographies of values are thresholded and the multiple comparison problem was addressed by the Benjamini-Hochberg procedure with a false discovery rate ($q$) thresholded at 0.05 (Benjamini and Hochberg, 1995).

### 2.10. Evaluation of motion control performance in resting-state recordings

After systematically evaluating the benefits of the bite bar and PCA-GLM algorithm, as an exploratory aim, we further combined these two approaches in the analysis of resting state data and compared with a conventional analysis without any motion control (i.e., between [Bite Bar, PCA-GLM] and [No Bite Bar, No Correction]). Since the focus of our study is on jaw-related motion artifacts, we focused on the connectivity seeded from one identified clenching channel. Also, considering the long-distance connectivity was known for being erroneously affected by motion (Power et al., 2012), we then focused on comparing the cross-hemispheric connectivity, i.e., between the auditory channel located on the left hemisphere and all channels on the right hemisphere. Since both fNIRS and fMRI measure similar hemodynamic activities, we followed the fMRI protocol to quantify the resting state functional connectivity of fNIRS (Fox et al., 2005). Specifically, the Pearson's correlation coefficients were calculated between pairs of fNIRS channels and then converted to z scores by the Fisher's Z-transformation. To assess whether functional connectivity was significant at the group level, a two-tailed one-sample t-test was performed. Then to assess whether applying the bite bar and the PCA-GLM method have made any differences, a two-tailed, paired t-test was performed between the conditions of [Bite Bar, PCA-GLM] vs. [No Bite Bar, No Correction]. The multiple comparison problem was addressed by the Benjamini-Hochberg procedure with a false discovery rate ($q$) thresholded at 0.05 (Benjamini and Hochberg, 1995).

## 3. Results

### 3.1. Effects of jaw motion on fNIRS signals

Fig. 2 shows the entire time courses, block averages and topographies of HbO during the clenching task. Based on the group-level topography, Channel #3 and Channel #30 over the left and right temporalis muscles, respectively, were designated as the clenching channels. The relative concentration changes in bilateral clenching channels exhibit temporally structured and consistent fluctuations across seven consecutive blocks in a representative session (Fig. 2A) and across the group (Fig. 2B), which appear like hemodynamic responses. The block averages modulated by the jaw clenching showed an increase in HbO, highly resembling the response evoked by a motor task (Zhang et al., 2021) or an auditory task (Luke et al., 2021), yet with a larger amplitude. Interestingly, the peaks in HbO caused by each of the three individual jaw-clenching movements are visible in the block averages. Figs. 2C and 2D show the topographies of the mean amplitudes averaged from 5 s to 15 s. The topographies of the artifacts caused by jaw clenching exhibit a broad spatial extent within the montage, primarily covering the left and right auditory cortices and extending over the parietal and frontal cortices. Meanwhile, the task-evoked HbR responses as decreases resemble typical deoxygenated hemoglobin responses to sound stimuli over the auditory cortices (shown in Supplemental Fig. 1).

The entire time courses and block averages of HbO in the identified clenching channels (Channel #3 is the left clenching channel and Channel #30 is the right clenching channel) are plotted at the session level (A) and group level (B). Topographies of amplitudes averaged from

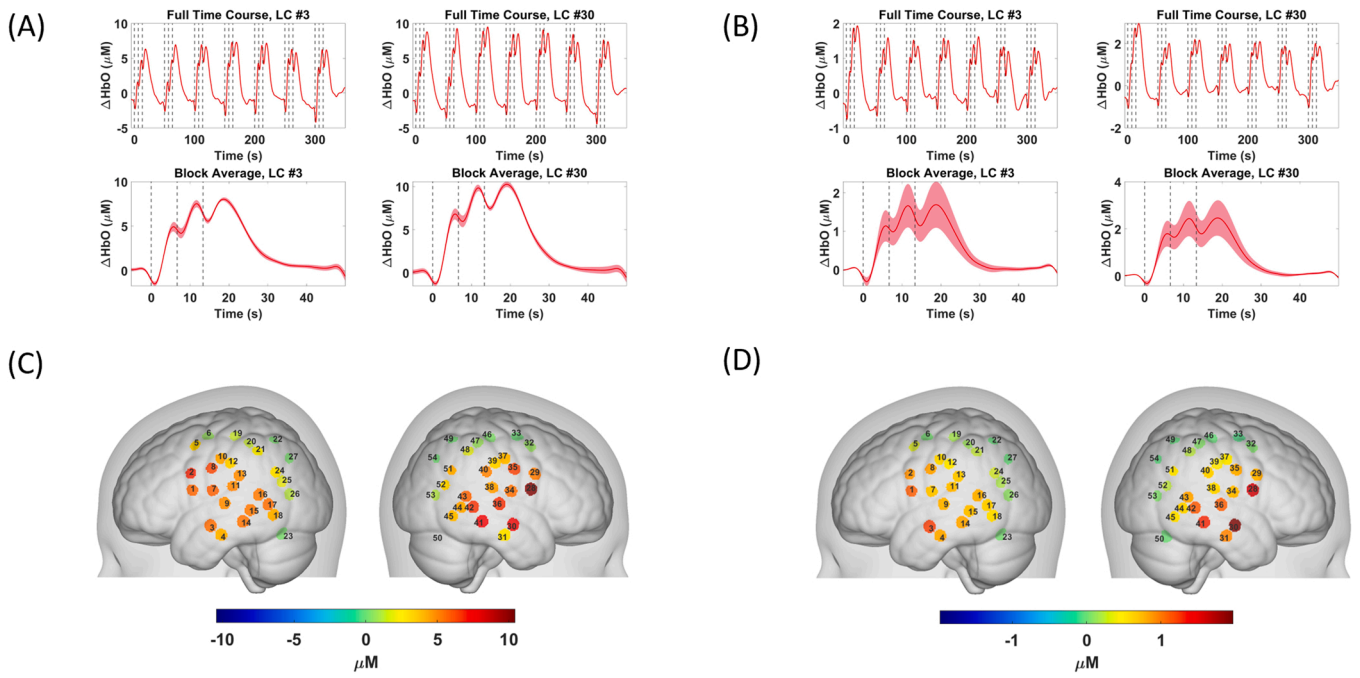


**Fig. 2.** Task-evoked-like fluctuations in HbO caused by jaw clenching.

5 s to 15 s of all LS channels are shown at the session level (C) and group level (D). The shaded areas of red color represent the standard errors across blocks in a single session (A) and across the group (B).

In order to quantify the motion-related artifacts, Fig. 3A shows the group-level GVTD measure at the clenching condition. The time course of GVTD highly resembles the full time course in the clenching channel shown in Fig. 2B, both exhibiting on and off fluctuations across seven consecutive blocks. Fig. 3B shows that at the clenching task, the mean GVTD during the movement period (0–20 s) is significantly higher than that during the resting period (20–50 s), which confirms that these global fluctuations across channels are signatures of the jaw clenching.

(A) shows the group-level GVTD time courses during the clenching task. The dash lines indicate the visually cued jaw clenching movements that subjects were instructed to perform. (B) plots the mean and standard errors of GVTD values during the movement period and the resting period at the clenching task. (C) and (D) plot the mean and standard errors of GVTD values across the entire session without and with a customized bite bar addressed to each subject at the auditory task (C) and the resting state (D). The asterisk ** indicates significant differences in the two-tailed paired-sample t-test at $p < 0.01$.

Furthermore, we have investigated the spatio-temporal pattern of the fNIRS signals during the jaw-clenching movements, in order to examine the prerequisites for the PCA-GLM denoising algorithm. The outcomes of PCA on one single session's data (the same session as in Fig. 2A) are illustrated as an example in Fig. 4. Fig. 4A shows the variance percentage accounted for by each component in the data of LS channels. After applying PCA on the LS recording acquired at the clenching task, a prominent component was identified such that the PC-LS component explained more than 95 % of the total variance in the data, which is also observed in other sessions. The time course of PC-LS is shown in Fig. 4B, which highly resembles the entire time course shown in Fig. 2A and is consistent with the high GVTD measure in Fig. 3A. Moreover, the noise component PC-LS presents a homogenous topographic distribution located over the temporalis muscle region (Fig. 4C), indicating a high coefficient of spatial uniformity, which is a prerequisite for the success of the denoising PCA-GLM method (Zhang et al., 2021). In all individuals, PC-LS presents an overall CSU of 2.88 ± 1.02 (mean ± SD), ranging from 0.99 to 7.47 (specifically, for the conditions with a bite bar, CSU = 2.94 ± 1.10/mean ± SD and ranged from 0.99 to 7.47; for the conditions without a bite bar, CSU = 2.82 ± 0.94/mean ± SD and ranged from 1.03 to 5.22). In comparison, the CSU obtained from the voluntary clenching condition is also at a consistent, high level in the same montage, with CSU value of 2.22 ± 1.04 (mean ± SD) and ranging from 1.00 to 4.44.

(A) Variance explained by components in PCA. (B) The time course of PC-LS captures the jaw movements. (C) The topography of PC-LS presents spatial uniformity.

### 3.2. Controlling jaw-related motion artifacts in auditory tasks

The motion artifacts, as quantified by GVTD, are significantly reduced using a bite bar during the auditory task than without a bite bar (Fig. 3C). This indicates that the individually customized bite bar proposed in this study is effective in suppressing jaw clenching movements and thus reducing global fluctuations in the fNIRS signals. Fig. 5A shows group-level auditory responses after controlling the jaw-movement-related artifacts, i.e., using a bite bar and the de-noising PCA-GLM method. The topography in Fig. 5A presents the auditory-evoked response by comparing the mean amplitude of the block averages during the stimulus window (5–18 s) to that during the silence window (20–30 s). There are several activated channels in both hemispheres while Channel #3 located over the left middle temporal gyrus is the most activated. Channel #3 was therefore identified as the auditory channel in the following analyses. Noteworthy, the auditory channel has previously been identified as the clenching channel (Fig. 2). In addition, Channel #25, which is located over the temporal-parietal junction and expected to *not* show any stimuli-related activations, serves as a non-auditory-related control channel.

In order to determine the benefits of motion control in measuring auditory responses, two-way ANOVA evaluated four performance metrics regarding the bite bar and the PCA-GLM method, in the auditory channel (Channel #3, located over the middle temporal gyrus) and the control channel (Channel #25, located over the temporal-parietal junction), separately. Figs. 5B and 5C illustrate the time courses of block averages under four different conditions of the two-way ANOVA, including No Bite Bar & No Correction, Bite Bar & No Correction, No Bite Bar & PCA-GLM and Bite Bar & PCA-GLM. In Channel #3 (Fig. 5B), the block averages with a bite bar exhibit increases in HbO that last during

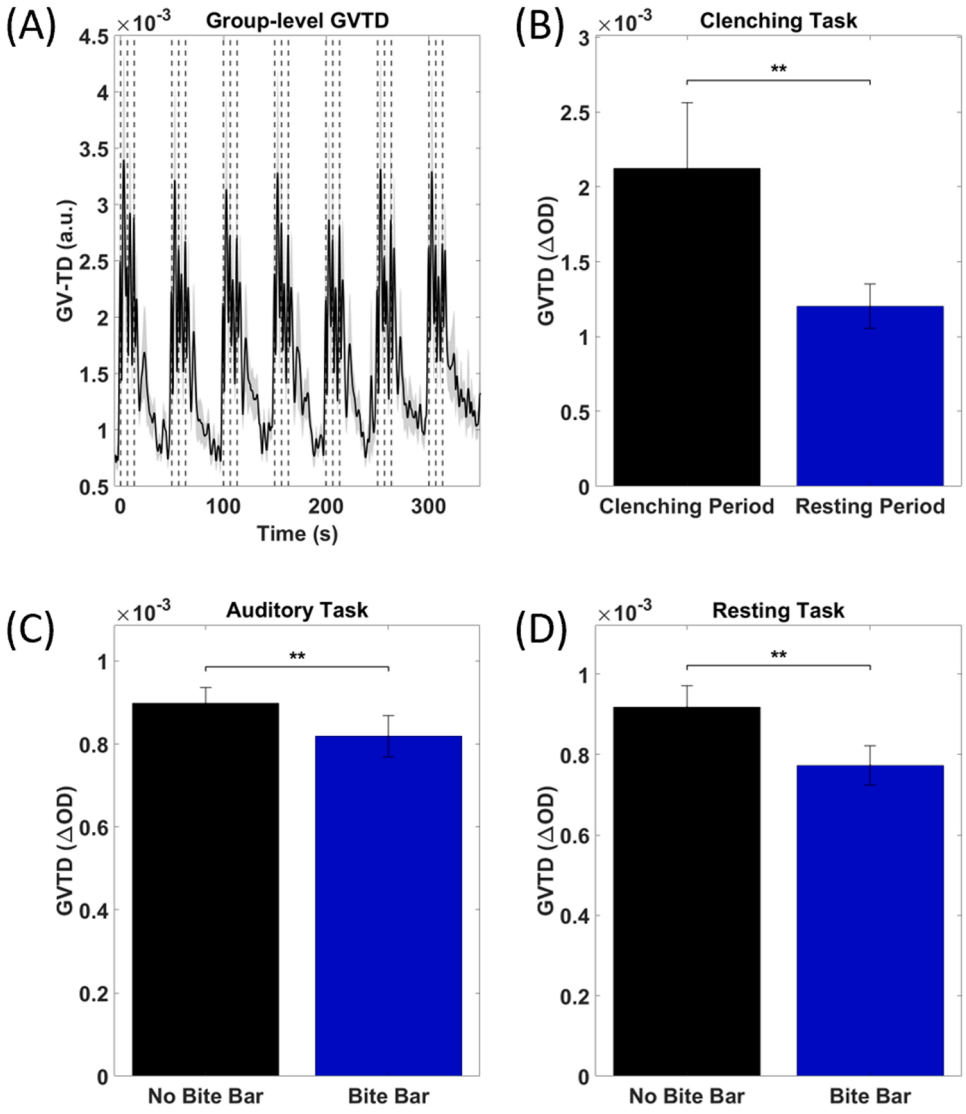


**Fig. 3.** Global variance of temporal derivatives (GVTD) measure motion artifacts in fNIRS.

and shortly after the stimulus window, as a typical positive auditory-evoked response. In Channel #25 (Fig. 5C), the block averages show decreases in HbO response without PCA-GLM, regardless of whether a bite bar was applied. Such decrease in HbO in the regions near the auditory cortex could be attributed to a nonneuronal origin, i.e., cortical blood stealing (Harel et al., 2002; Shmuel et al., 2002). Interestingly, after PCA-GLM is applied, the control Channel #25 shows an almost flattened response. The two-way ANOVA analysis revealed that the effect of a bite bar was significant in the auditory channel (Fig. 5B), whereas the effect of PCA-GLM method was significant in the non-auditory channel (Fig. 5C). Post-hoc analysis regarding the bite-bar effect shows that the beta value, CNR and mean amplitude are significantly increased, while within-subject SD is decreased with a bite bar applied (Fig. 5B). Meanwhile, Fig. 5C shows the post-hoc results regarding the effect of PCA-GLM. No Correction presents negative values in the beta value, CNR and mean amplitude, which indicate decreases in HbO (i.e., negative HbO response) in a non-auditory channel. However, after applying PCA-GLM these negative values are corrected to be near zero values. The within-subject SD is again significantly lowered after PCA-GLM. These results suggest that a bite bar improves the HbO response of activations in the auditory-related channel, while PCA-GLM corrects the negative HbO response in the non-auditory-related control channel.

(A) Auditory-evoked response map ($q < 0.05$, multiple comparisons corrected). (B) Comparison of block averages under four different conditions in Channel #3, a representative clenching channel and also an auditory channel. (C) Comparison of block averages under four different conditions in Channels #25, a non-auditory-related control channel. The gray shaded areas indicate the auditory stimuli period. Shaded areas on the curves of colors indicated standard errors. Quantitative metrics for evaluation include the beta value, mean amplitude during the task period, contrast-to-noise ratio (CNR), and within-subject SD. * indicates $p < 0.05$ and *** indicates $p < 0.001$ in post-hoc analysis.

In addition to evaluating a few channels of interest noted above, a topographic presentation of improvement in all channels is illustrated in Fig. 6. Interestingly, the channels of the bite-bar effect and the PCA-GLM effect do not overlap, suggesting these two approaches of controlling motion artifacts are complementary to each other. Regarding the effect of a bite bar, the channels over the left or right middle temporal cortex show a reduced within-subject SD (Fig. 6A), an enhanced HbO activations (Fig. 6E) and taken together, an overall increased CNR (Fig. 6C), which are attributed to using a bite bar. In the meantime, the PCA-GLM has led to likewise reduced within-subject SD (Fig. 6B), which however is in the channels that centered at the parietal-temporal junction and spanned across temporal, parietal and frontal cortices. In addition, in those channels over non-auditory-related regions that showed negative

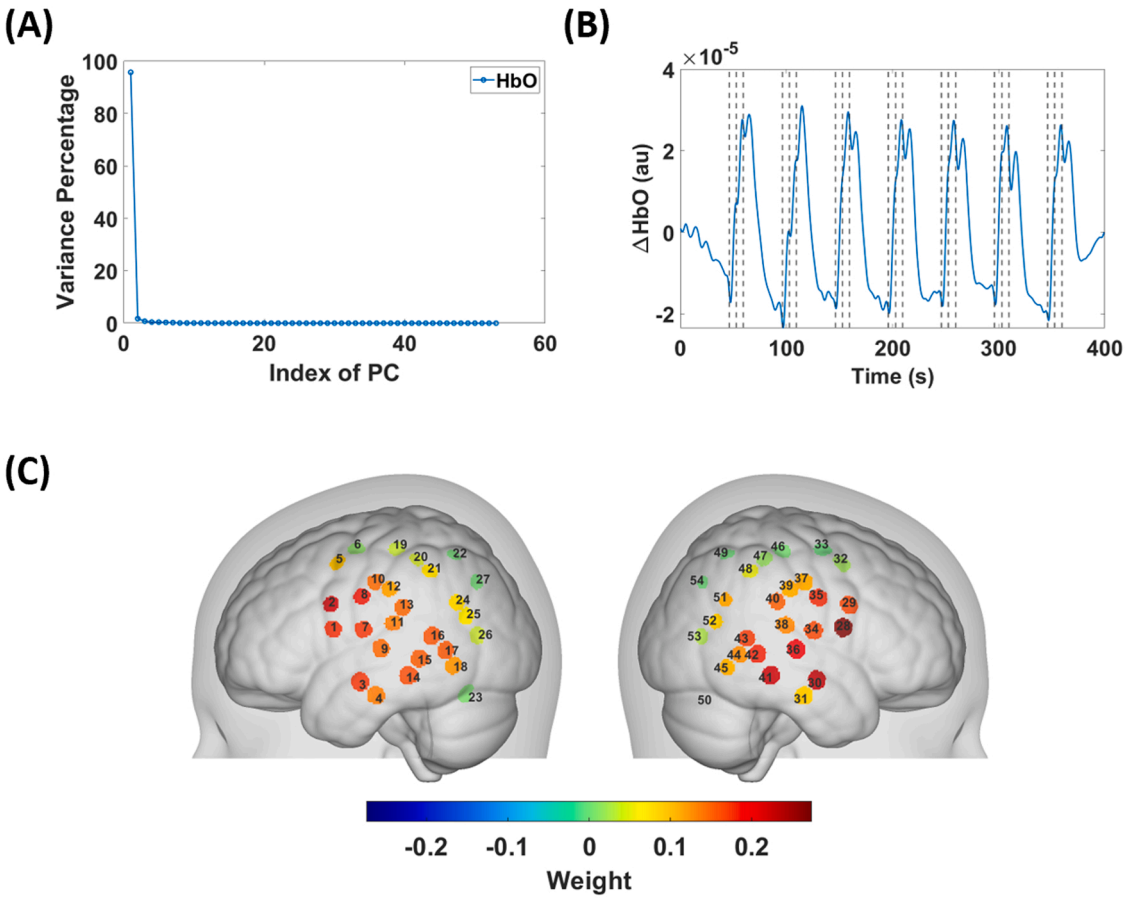


**Fig. 4.** Spatio-temporal pattern of the fNIRS signals during clenching task.

HbO responses, applying PCA-GLM has corrected the negative values to near-zero values. Therefore, the effect of PCA-GLM on the non-auditory-related channels is exhibited as increases in CNR and beta values (Figs. 6F and 6D, respectively).

Four evaluation metrics are calculated, including within-subject SD (A, B), contrast-to-noise ratio (C, D), and beta value of the GLM regressor for auditory stimuli (E, F). Comparisons are made between bite-bar vs. no-bite-bar (A, C, E), and PCA-GLM vs. without-correction (B, D, F). Only channels with significant differences at comparison ($p < 0.05$) are shown. * indicates channels with a significant difference after multiple comparisons correction ($q < 0.05$). Red-yellow colorbar visualizes increase of metric values, and blue-green colorbar visualizes decrease of metric values.

### 3.3. *Controlling jaw-related motion artifacts during resting state*

Fig. 3D shows that during the resting task, the mean GVTD across the entire session is significantly reduced with a bite bar applied to each subject than without a bite bar. Fig. 7A and B show the functional connectivity seeded at Channel #3 (the identified clenching channel and also identified as the auditory channel) in the conditions of [No Bite Bar, No Correction] and [Bite Bar, PCA-GLM], respectively. Fig. 7C shows the differences in functional connectivity between [Bite Bar, PCA-GLM] and [No Bite Bar, No Correction]. There is significantly increased connectivity between Channel #3 in the left hemisphere and Channels #30, #36 and #41 in the right hemisphere, which are located at the symmetric and near-symmetric locations over the middle temporal gyrus. Using a combination of the bite bar and PCA-GLM algorithm has enhanced the cross-hemisphere functional connectivity between homologous auditory cortices.

## 4. Discussion

With the advantages of portability, cost-effectiveness, low operating noise and compatibility with electronic or magnetic stimulation devices (Chiarelli et al., 2017; Luke et al., 2021; Scholkmann et al., 2014), fNIRS has seen increasing applications in studying hearing, language and cognitive functions (Sevy et al., 2010; Wan et al., 2018). Especially, recent development of fNIRS offers new capability of imaging the brain-wide resting state functional connectivity (Khan et al., 2022, 2021; Zhang et al., 2022a). However, there are still important confounding factors in fNIRS signals that should be controlled or addressed, including interferences from superficial layers of the head, systemic physiological noises and motion artifacts (von Lühmann et al., 2019, 2020; Zhang et al., 2021). Although less vulnerable to head movements, fNIRS signals are affected by jaw movements, such as teeth clenching that occurs voluntarily or involuntarily, which causes contractions of the temporalis muscle (Novi et al., 2020; Schecklmann et al., 2017). The jaw movements could result in blood flow changes in the temporalis muscle as well as relative movements between the optodes and the scalp, leading to artifacts in the fNIRS signals (Schecklmann et al., 2017). Although many previous studies have investigated the rigid form of head motion (Cui et al., 2010; Fishburn et al., 2019; Izzetoglu et al., 2010; Scholkmann et al., 2010), the issue of jaw motion in fNIRS recordings remains largely unaddressed. Recent development by Novi et al. (2020) has introduced algorithms of spline interpolation and wavelet decomposition to suppress the motion artifacts elicited during a speech protocol. However, the spontaneous and asynchronous artifacts related to jaw motion remain an uncontrolled issue in fNIRS research, which could sabotage the data quality substantially. Indeed, our results have shown that voluntary jaw clenching can introduce artifacts that resemble the task-evoked responses in motor and auditory tasks. Specifically, the jaw

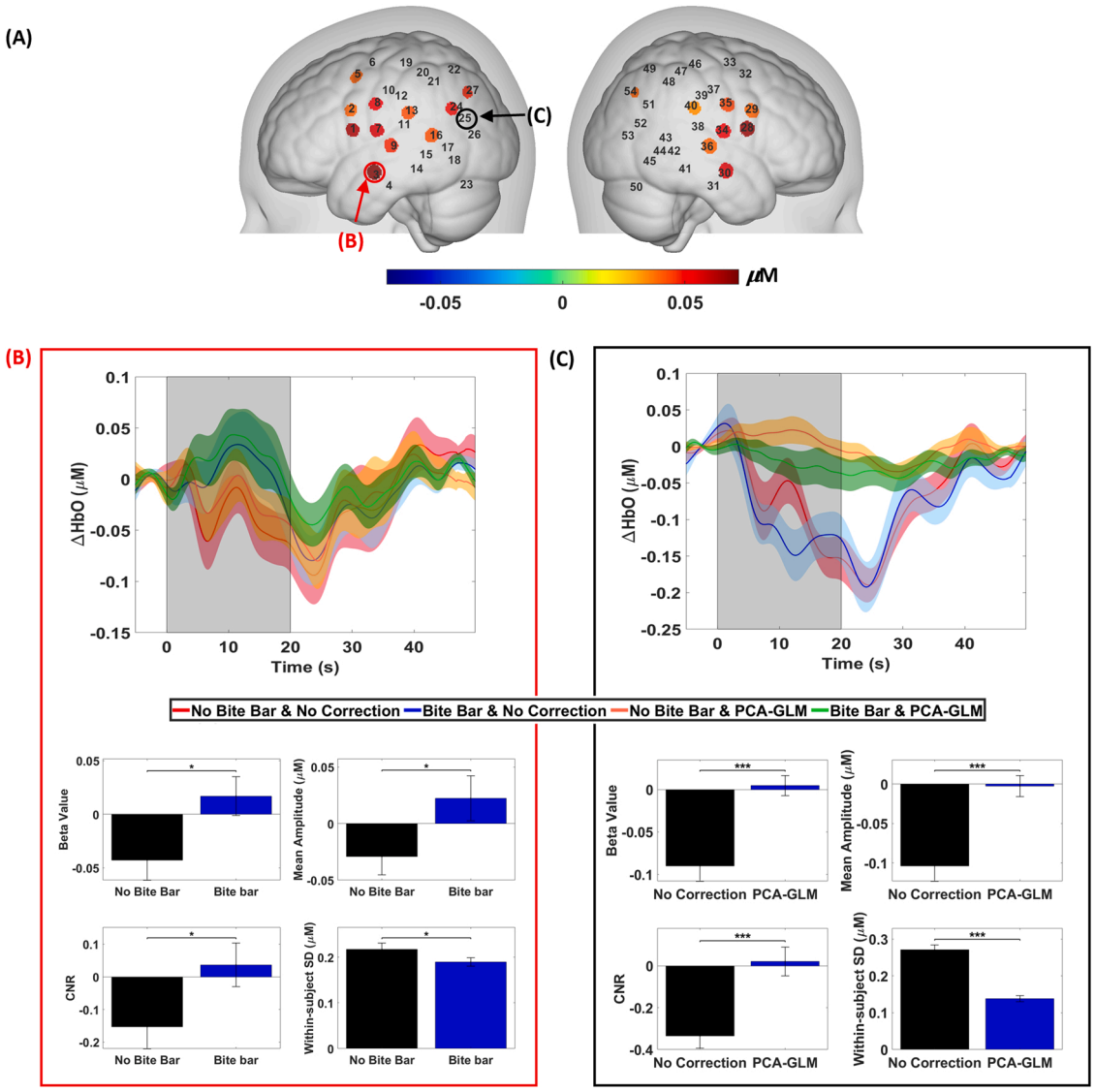


**Fig. 5.** Improvements in HbO auditory responses by the bite bar and PCA-GLM.

clenching introduces a task-activation-like increase in HbO (Fig. 2B) coupled with a typical decrease in HbR (Supplemental Fig. 1B), which is consistent with the previous literature (Novi et al., 2020; Schecklmann et al., 2017) and our pilot investigation (Zhang et al., 2022b). Noteworthy, the clenching channel identified to show the most prominent artifacts in our study was identified as a representative auditory channel, as well. Therefore, these jaw-related motion artifacts could be easily misinterpreted as auditory evoked responses and lead to spurious interpretation in the hearing, language and other cognitive functions. In addition, the jaw-movement-related artifacts are not affecting only one or two channels, but instead exhibit a large, symmetric pattern over the bilateral auditory cortices and extend to parietal and frontal/prefrontal regions (shown in Fig. 2D and Supplemental Fig. 1D), which are the cortical tissues underneath the temporalis muscles. Additional results of GVTD, a measure of the coherent fluctuations across all recorded channels to quantify the motion, attested to globally higher magnitude during the clenching period than during the resting period (Figs. 3A and 3B). Since fNIRS measurements depend on the tissue absorption and scattering of the near-infrared light along the penetrating path, the signal originated from temporalis muscles is inevitably superimposed to any signal from the deeper cortex. The extended area affected by jaw-related motion artifacts calls for caution in studies that not only involve auditory cortex but also a greater domain that includes the parietal and the frontal/prefrontal lobes.

Importantly, although both oxygenation status in the temporalis muscle and the optode displacement could contribute to the measured motion artifacts in fNIRS, the antagonistic presentation of the data (i.e., HbO increase and HbR decrease concurrently measured at the channels) points out that the clenching-related artifacts is dominantly contributed by the metabolic and hemodynamic processes. Otherwise, the optode displacement would likely have led to concurrent HbO and HbR changes in the same direction of increases/decreases (Cui et al., 2010). Thus, these jaw-related motion artifacts as opposite fluctuations in HbO and HbR would remain uncorrected in algorithms that are designed for correcting same-direction changes in HbO and HbR (Cui et al., 2010). The data from our study have therefore underlined the importance of new strategies to control, detect and remove the jaw clenching artifacts in fNIRS recordings.

In order to control the jaw movements during the recordings and therefore prevent the motion artifacts from happening in the first place, we designed a novel bite bar consisting of a rectangle plastic plate and vinyl polysiloxane putty customized for each participant (Fig. 1). The use of a bite bar has been commonly practiced in neuroscience research, especially in tasks demanding stringent motion control (Menon et al.,

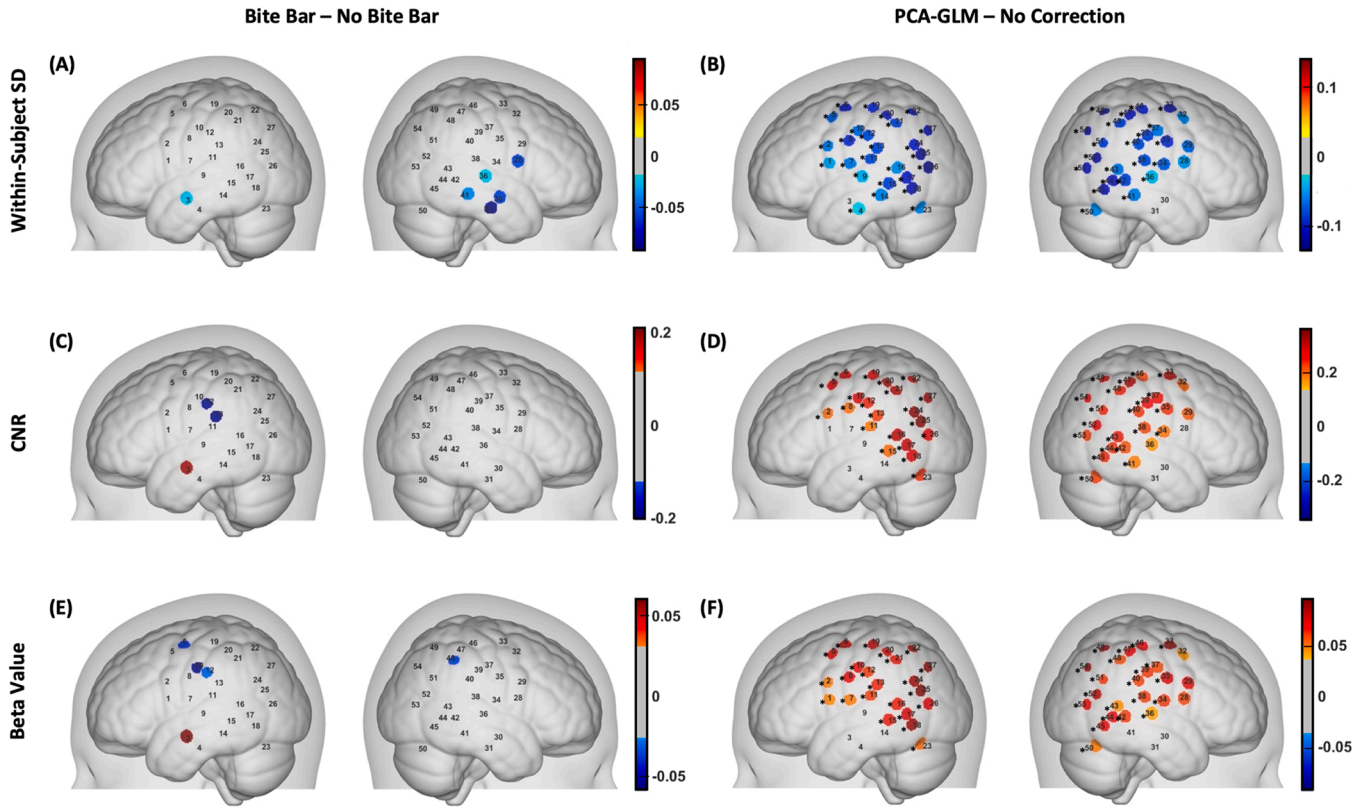


**Fig. 6.** Topographies of improvements in fNIRS auditory responses by a bite bar and PCA-GLM.

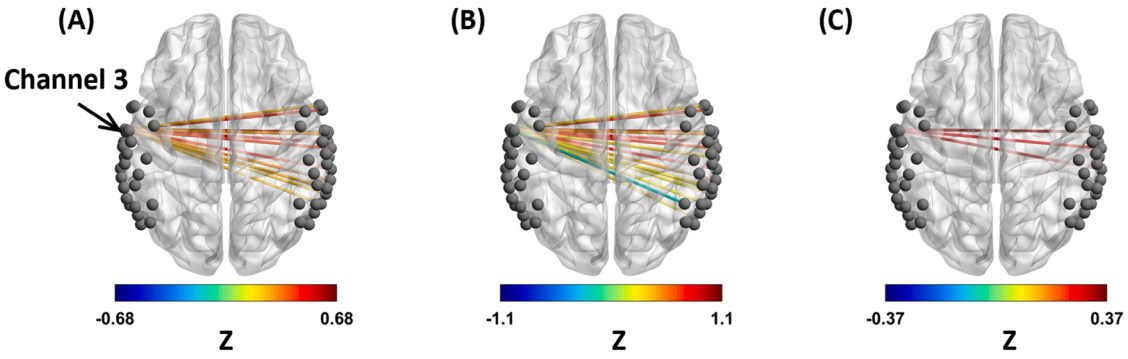


**Fig. 7.** Enhanced cross-hemisphere resting-state functional connectivity by a bite bar and PCA-GLM. (A) and (B) show functional connectivity seeded at Channel #3 with [No Bite Bar, No correction] and [Bite Bar, PCA-GLM], respectively. (C) shows the differences in functional connectivity, [Bite Bar, PCA-GLM] subtracting [No Bite Bar, No correction]. The strength of functional connectivity is color-coded. The line connecting two channels indicates significant functional connectivity in (A) and (B) and differences in (C) ($q < 0.05$, multiple comparisons corrected).

1997; Engel et al., 1997). While many earlier studies have emphasized the fixation of head position when using a bite bar that is attached to other equipment, such as MRI coils (Menon et al., 1997; Engel et al., 1997), our design of the bite bar was mainly for controlling voluntary jaw movements. Therefore, the subjects in our study were instructed to bite on the putty during the entire recording, while sitting comfortably without their head positions being fixed. The results showed that the mean GVTD during the entire session is significantly lower while a bite bar is applied to each subject at both the auditory and resting tasks (Figs. 3C and 3D), which indicates that the individually customized bite bar is effective in suppressing the jaw clenching movements and reducing the artifacts across channels. The time courses of HbO (Fig. 5) and HbR (Supplemental Fig. 2) in the auditory channel show a signature increase in HbO and decrease in HbR with a bite bar, while without the bite bar, the traces present significantly stronger fluctuations and the expected responses are less clear.

In addition to using a bite bar, we further explored whether a denoising algorithm could remove the artifacts in the fNIRS recordings. The homogeneous spatial pattern of the clench-related activities within the montage (Figs. 2C and 2D) and the consistent temporal profile of the fNIRS time course following the clenching behavior (Figs. 2A and 2B) warrant that a denoising method that exploits the spatial uniformity and variance of data would be able to correct the noise. Indeed, the identified noise component PC-LS shows a time course that well captured the jaw-clenching fluctuations (Fig. 4B) as well as a spatial pattern that concentrated over the temporalis muscle region (Fig. 4C). After applying PCA-GLM (Figs. 5 and 6), the entire time courses, block averages and topographies have shown largely reduced variance compared to those with No Correction, which demonstrates that PCA-GLM is effective in correcting the motion artifacts.

Furthermore, the PCA-GLM has also corrected the negative changes of HbO values in the parietal-temporal regions. Negative HbO response to auditory stimuli, i.e., relative decrease in HbO with respect to the baseline, has been noted in many previous fNIRS studies, especially in regions adjacent to but outside of the auditory cortices (Collins-Jones et al., 2021; Plichta et al., 2011; Steinmetzger et al., 2020). Meanwhile, those negative HbO responses are commonly observed with negative HbR responses in the same channels (Plichta et al., 2011) and accompanied by similar decreases in HbO in superficial measurements (Steinmetzger et al., 2020), which therefore were considered as physiological noises and not attributed to neuronal-related activities. Recently, a study by Steinmetzger et al., (2020) suggested that the negative HbO response is due to the so-called "cerebral blood steeling" phenomenon, which is a decrease in absolute blood flow and volume without underlying significant change in neuronal activity (Harel et al., 2002; Shmuel et al., 2002). Similar negative HbO responses were reported in the prefrontal region (Kirilina et al., 2012), too, which were demonstrated to be systemic artifacts due to a task-evoked sympathetic arterial vasoconstriction followed by a decrease in venous volume. Based on these observations, we consider that the noise component PC-SS derived from multi-channel superficial measurements in our study is a systematic artifact that originates from non-neuronal process. Thus, the correction of the negative HbO response by PCA-GLM is a reasonable and meritorious approach, resulting in near-zero values as expected in non-auditory channels.

Notably, a topographic evaluation on the performance of motion correction revealed that these two approaches - the bite bar and the denoising PCA-GLM algorithm - work complementary to each other in the way of correcting the jaw related artifacts originated from different regions (Fig. 6). While the bite bar is especially effective in increasing CNR and reducing variance in the clenching channel, the PCA-GLM is suited to remove the superficial activities that mask out an extended area of temporal, parietal and frontal/prefrontal cortices. The benefits can be combined, as evidenced in the auditory response (Fig. 5A) and the resting state functional connectivity (Fig. 7). The cross-hemisphere connectivity in auditory cortices have been replicated in our fNIRS study, which is consistent with prior discovery by electrophysiological recordings (Nir et al., 2008), fMRI (Cordes et al., 2000; Smith et al., 2009) and fNIRS (Eggebrecht et al., 2014; San Juan et al., 2017). Noteworthy, the combined approach of a bite bar and PCA-GLM denoising algorithm has strengthened the connectivity than the conventional method without any motion control, suggesting that our methodology could become a useful tool with higher sensitivity to investigate the diseases of hearing function, such as tinnitus where decreased connectivity between bilateral auditory cortices is seen as a hallmark of the diseased condition (Kim et al., 2012; San Juan et al., 2017).

Findings of our study suggest that both a bite bar and a denoising algorithm PCA-GLM, should be considered in fNIRS recordings acquired from a montage over auditory cortices. Participants in fNIRS studies should be instructed to refrain from any form of jaw movements during the recordings, such as clenching jaws, swallowing, speaking, chewing gum, etc. A bite bar, as an individually customized apparatus in this study, is encouraged for suppressing all kinds of jaw motions. However, if a study inevitably invites jaw motions, such as a speech protocol, the bite bar may not be applicable and the fNIRS data should be carefully handled to avoid motion artifacts being misinterpreted as neuronal activations (Novi et al., 2020). In addition, our study suggests that applying the PCA-GLM is beneficial for experiment datasets that are acquired with or without a bite bar. Noteworthy, the analytic denoising by PCA-GLM does *not* require any jaw clenching data in addition to the experimental paradigm. For fNIRS data acquired in partial montage centered at the auditory cortices, our study recommends PCA-GLM removing one noise component is sufficient and effective. Although the algorithm is automatic, the CSU of the noise component PC-LS should have a value of above 1 (good), or at least 0.5 (acceptable). Meanwhile, for a whole-head montage that covers extensively beyond the auditory cortices, it is possible that more than one noise comments could be removed, which however, warrants a systematical investigation in a future study.

## 5. Conclusions

In summary, we have characterized the effects of jaw motion on fNIRS recordings, developed an individually customized bite bar to suppress the movements, and validated our previously established PCA-GLM method in removing jaw-related motion artifacts. This study underlines the importance of controlling the jaw motion and provides a solution that integrates a bite bar in the experimental stage and PCA-GLM in the data processing stage. The characterization of motion artifacts and the validation of a problem-solving strategy presented in our work will benefit the studying of hearing, language and cognitive functions in normal healthy subjects and patients.

## CRediT authorship contribution statement

FZ developed the method, collected and analyzed the data, and wrote the manuscript. AR designed the customized bite bar, collected and analyzed the data, and wrote the manuscript. AJ collected the data. LD designed the study and wrote the manuscript. HY designed the study, analyzed the data and wrote the manuscript.

## Conflict of interests

The authors declare no conflict of interest.

## Data availability

Data used in this study are not publicly available due to research data sharing restrictions from the IRB but are available from the corresponding author through a data use agreement.

## Acknowledgments

This work was supported by the National Science Foundation (RII Track-2 FEC 1539068, RII Track-4 2132182), National Institute of General Medical Sciences (P20GM135009), and Undergraduate Research Opportunities Program of The University of Oklahoma, Norman, OK.

## Appendix A. Supporting information

Supplementary data associated with this article can be found in the online version at doi:10.1016/j.jneumeth.2023.109810.

## References

Benjamini, Y., Hochberg, Y., 1995. Controlling the false discovery rate: a practical and powerful approach to multiple testing. J. R. Stat. Soc.: Ser. B (Methodol. ) 57, 289–300.

Bortfeld, H., 2019. Functional near-infrared spectroscopy as a tool for assessing speech and spoken language processing in pediatric and adult cochlear implant users. Dev. Psychobiol. 61, 430–443.

Brigadoi, S., Ceccherini, L., Cutini, S., Scarpa, F., Scatturin, P., Selb, J., Gagnon, L., Boas, D.A., Cooper, R.J., 2014. Motion artifacts in functional near-infrared spectroscopy: a comparison of motion correction techniques applied to real cognitive data. Neuroimage 85, 181–191.

Chen, L.-C., Sandmann, P., Thorne, J.D., Herrmann, C.S., Debener, S., 2015. Association of concurrent fNIRS and EEG signatures in response to auditory and visual stimuli. Brain Topogr. 28, 710–725.

Chiarelli, A.M., Zappasodi, F., Di Pompeo, F., Merla, A., 2017. Simultaneous functional near-infrared spectroscopy and electroencephalography for monitoring of human brain activity and oxygenation: a review. Neurophotonics 4, 041411.

Collins-Jones, L.H., Cooper, R.J., Bulgarelli, C., Blasi, A., Katus, L., McCann, S., BRIGHT Study Team, 2021. Longitudinal infant fNIRS channel-space analyses are robust to

variability parameters at the group-level: An image reconstruction investigation. NeuroImage 237, 118068.
Cordes, D., Haughton, V.M., Arfanakis, K., Wendt, G.J., Turski, P.A., Moritz, C.H., Quigley, M.A., Meyerand, M.E., 2000. Mapping functionally related regions of brain with functional connectivity MR imaging. Am. J. Neuroradiol. 21, 1636–1644.
Cui, X., Bray, S., Reiss, A.L., 2010. Functional near infrared spectroscopy (NIRS) signal improvement based on negative correlation between oxygenated and deoxygenated hemoglobin dynamics. Neuroimage 49, 3039–3046.
Eggebrecht, A.T., Ferradal, S.L., Robichaux-Viehoever, A., Hassanpour, M.S., Dehghani, H., Snyder, A.Z., Hershey, T., Culver, J.P., 2014. Mapping distributed brain function and networks with diffuse optical tomography. Nat. Photonics 8, 448–454.
Fishburn, F.A., Ludlum, R.S., Vaidya, C.J., Medvedev, A.V., 2019. Temporal derivative distribution repair (TDDR): a motion correction method for fNIRS. Neuroimage 184, 171–179.
Fox, M.D., Snyder, A.Z., Vincent, J.L., Corbetta, M., Van Essen, D.C., Raichle, M.E., 2005. The human brain is intrinsically organized into dynamic, anticorrelated functional networks. Proc. Natl. Acad. Sci. USA 102, 9673–9678.
Harel, N., Lee, S.P., Nagaoka, T., Kim, D.S., Kim, S.G., 2002. Origin of negative blood oxygenation level-dependent fMRI signals. J. Cereb. Blood Flow. Metab. 22, 908–917.
Herold, F., Wiegel, P., Scholkmann, F., Müller, N.G., 2018. Applications of functional near-infrared spectroscopy (fNIRS) neuroimaging in exercise–cognition science: a systematic, methodology-focused review. J. Clin. Med. 7, 466.
Hou, X., Zhang, Z., Zhao, C., Duan, L., Gong, Y., Li, Z., Zhu, C., 2021. NIRS-KIT: a MATLAB toolbox for both resting-state and task fNIRS data analysis. Neurophotonics 8, 010802.
Huppert, T.J., Diamond, S.G., Franceschini, M.A., Boas, D.A., 2009. HomER: a review of time-series analysis methods for near-infrared spectroscopy of the brain. Appl. Opt. 48, D280–D298.
Izzetoglu, M., Chitrapu, P., Bunce, S., Onaral, B., 2010. Motion artifact cancellation in NIR spectroscopy using discrete Kalman filtering. Biomed. Eng. Online 9, 16.
Khan, A.F., Zhang, F., Yuan, H., Ding, L., 2021. Brain-wide functional diffuse optical tomography of resting state networks. J. Neural Eng. 18.
Khan, A.F., Zhang, F., Shou, G., Yuan, H., Ding, L., 2022. Transient brain-wide coactivations and structured transitions revealed in hemodynamic imaging data. Neuroimage 260, 119460.
Kim, J.Y., Kim, Y.H., Lee, S., Seo, J.H., Song, H.J., Cho, J.H., Chang, Y., 2012. Alteration of functional connectivity in tinnitus brain revealed by resting-state fMRI? A pilot study. Int J. AudioL 51, 413–417.
Kirilina, E., Jelzow, A., Heine, A., Niessing, M., Wabnitz, H., Brühl, R., Tachtsidis, I., 2012. The physiological origin of task-evoked systemic artefacts in functional near infrared spectroscopy. Neuroimage 61 (1), 70–81.
Kohno, S., Miyai, I., Seiyama, A., Oda, I., Ishikawa, A., Tsuneishi, S., Amita, T., Shimizu, K., 2007. Removal of the skin blood flow artifact in functional near-infrared spectroscopic imaging data through independent component analysis. J. Biomed. Opt. 12, 062111.
Lindquist, M.A., Loh, J.M., Atlas, L.Y., Wager, T.D., 2009. Modeling the hemodynamic response function in fMRI: efficiency, bias and mis-modeling. Neuroimage 45, S187–S198.
von Lühmann, A., Boukouvalas, Z., Müller, K.-R., Adalı, T., 2019. A new blind source separation framework for signal analysis and artifact rejection in functional near-infrared spectroscopy. NeuroImage 200, 72–88.
von Lühmann, A., Li, X., Müller, K.-R., Boas, D.A., Yücel, M.A., 2020. Improved physiological noise regression in fNIRS: a multimodal extension of the general linear model using temporally embedded canonical correlation analysis. NeuroImage 208, 116472.
Luke, R., Larson, E., Shader, M.J., Innes-Brown, H., Van Yper, L., Lee, A.K.C., Sowman, P. F., McAlpine, D., 2021. Analysis methods for measuring passive auditory fNIRS responses generated by a block-design paradigm. Neurophotonics 8, 025008.
Maidan, I., Nieuwhof, F., Bernad-Elazari, H., Reelick, M.F., Bloem, B.R., Giladi, N., Deutsch, J.E., Hausdorff, J.M., Claassen, J.A., Mirelman, A., 2016. The role of the frontal lobe in complex walking among patients with Parkinson's disease and healthy older adults: an fNIRS study. Neurorehabil. Neural Repair 30, 963–971.
Makizako, H., Shimada, H., Park, H., Tsutsumimoto, K., Uemura, K., Suzuki, T., 2013. Brain activation during dual-task walking and executive function among older adults with mild cognitive impairment: a fNIRS study. Aging Clin. Exp. Res. 25, 539–544.
Nguyen, H.-D., Yoo, S.-H., Bhutta, M.R., Hong, K.-S., 2018. Adaptive filtering of physiological noises in fNIRS data. Biomed. Eng. Online 17, 180.
Nir, Y., Mukamel, R., Dinstein, I., Privman, E., Harel, M., Fisch, L., Gelbard-Sagiv, H., Kipervasser, S., Andelman, F., Neufeld, M.Y., Kramer, U., Arieli, A., Fried, I., Malach, R., 2008. Interhemispheric correlations of slow spontaneous neuronal fluctuations revealed in human sensory cortex. Nat. Neurosci. 11, 1100–1108.
Novi, S.L., Roberts, E., Spagnuolo, D., Spilsbury, B.M., Price, D.C., Imbalzano, C.A., Forero, E., Yodh, A.G., Tellis, G.M., Tellis, C.M., Mesquita, R.C., 2020. Functional near-infrared spectroscopy for speech protocols: characterization of motion artifacts and guidelines for improving data analysis. Neurophotonics 7, 015001.
Piper, S.K., Krueger, A., Koch, S.P., Mehnert, J., Habermehl, C., Steinbrink, J., Obrig, H., Schmitz, C.H., 2014. A wearable multi-channel fNIRS system for brain imaging in freely moving subjects. Neuroimage 85, 64–71.
Plichta, M.M., Gerdes, A.B., Alpers, G.W., Harnisch, W., Brill, S., Wieser, M.J., Fallgatter, A.J., 2011. Auditory cortex activation is modulated by emotion: a functional near-infrared spectroscopy (fNIRS) study. Neuroimage 55 (3), 1200–1207.
Pollonini, L., Olds, C., Abaya, H., Bortfeld, H., Beauchamp, M.S., Oghalai, J.S., 2014. Auditory cortex activation to natural speech and simulated cochlear implant speech measured with functional near-infrared spectroscopy. Hear Res 309, 84–93.
Power, J.D., Barnes, K.A., Snyder, A.Z., Schlaggar, B.L., Petersen, S.E., 2012. Spurious but systematic correlations in functional connectivity MRI networks arise from subject motion. Neuroimage 59 (3), 2142–2154.
Saliba, J., Bortfeld, H., Levitin, D.J., Oghalai, J.S., 2016. Functional near-infrared spectroscopy for neuroimaging in cochlear implant recipients. Hear. Res. 338, 64–75.
San Juan, J., Hu, X.S., Issa, M., Bisconti, S., Kovelman, I., Kileny, P., Basura, G., 2017. Tinnitus alters resting state functional connectivity (RSFC) in human auditory and non-auditory brain regions as measured by functional near-infrared spectroscopy (fNIRS). PLOS One 12, e0179150.
Schecklmann, M., Mann, A., Langguth, B., Ehlis, A.-C., Fallgatter, A.J., Haeussinger, F.B., 2017. The temporal muscle of the head can cause artifacts in optical imaging studies with functional near-infrared spectroscopy. Front. Hum. Neurosci. 11, 456.
Scholkmann, F., Spichtig, S., Muehlemann, T., Wolf, M., 2010. How to detect and reduce movement artifacts in near-infrared imaging using moving standard deviation and spline interpolation. Physiol. Meas. 31, 649–662.
Scholkmann, F., Kleiser, S., Metz, A.J., Zimmermann, R., Mata Pavia, J., Wolf, U., Wolf, M., 2014. A review on continuous wave functional near-infrared spectroscopy and imaging instrumentation and methodology. Neuroimage 85 (Pt 1), 6–27.
Sevy, A.B., Bortfeld, H., Huppert, T.J., Beauchamp, M.S., Tonini, R.E., Oghalai, J.S., 2010. Neuroimaging with near-infrared spectroscopy demonstrates speech-evoked activity in the auditory cortex of deaf children following cochlear implantation. Hear Res 270, 39–47.
Sherafati, A., Snyder, A.Z., Eggebrecht, A.T., Bergonzi, K.M., Burns-Yocum, T.M., Lugar, H.M., Ferradal, S.L., Robichaux-Viehoever, A., Smyser, C.D., Palanca, B.J., 2020. Global motion detection and censoring in high-density diffuse optical tomography. Hum. Brain Mapp. 41, 4093–4112.
Shmuel, A., Yacoub, E., Pfeuffer, J., Van de Moortele, P.F., Adriany, G., Hu, X., Ugurbil, K., 2002. Sustained negative BOLD, blood flow and oxygen consumption response and its coupling to the positive response in the human brain. Neuron 36, 1195–1210.
Smith, S.M., Fox, P.T., Miller, K.L., Glahn, D.C., Fox, P.M., Mackay, C.E., Filippini, N., Watkins, K.E., Toro, R., Laird, A.R., Beckmann, C.F., 2009. Correspondence of the brain's functional architecture during activation and rest. Proc. Natl. Acad. Sci. USA 106, 13040–13045.
Steinmetzger, K., Shen, Z., Riedel, H., Rupp, A., 2020. Auditory cortex activity measured using functional near-infrared spectroscopy (fNIRS) appears to be susceptible to masking by cortical blood stealing. Hearing Research 396, 108069.
Strangman, G., Culver, J.P., Thompson, J.H., Boas, D.A., 2002. A quantitative comparison of simultaneous BOLD fMRI and NIRS recordings during functional brain activation. Neuroimage 17, 719–731.
Wan, N., Hancock, A.S., Moon, T.K., Gillam, R.B., 2018. A functional near-infrared spectroscopic investigation of speech production during reading. Hum. Brain Mapp. 39, 1428–1437.
Wu M., Wang Y., Zhao X., Xin T., Wu K., Liu H., Wu S., Lin M., Chai X., Li J. Anti-phasic oscillatory development for speech and noise processing in cochlear implanted toddlers. bioRxiv, 2022.
Xia, M., Wang, J., He, Y., 2013. BrainNet viewer: a network visualization tool for human brain connectomics. PloS One 8, e68910.
Zhang F., Reid A., Schroeder A., Cutter M., Kim K., Ding L., Yuan H. Clenching-Related Motion Artifacts in Functional Near-Infrared Spectroscopy in the Auditory Cortex. In: Proceedings of the Annu Int Conf IEEE Eng Med Biol Soc, 2022b; 2022: 4649–52.
Zhang, F., Cheong, D., Khan, A.F., Chen, Y., Ding, L., Yuan, H., 2021. Correcting physiological noise in whole-head functional near-infrared spectroscopy. J. Neurosci. Methods, 109262.
Zhang, F., Khan, A.F., Ding, L., Yuan, H., 2022a. Network organization of resting-state cerebral hemodynamics and their aliasing contributions measured by functional near-infrared spectroscopy. J. Neural Eng.
Zhang, Y., Brooks, D.H., Franceschini, M.A., Boas, D.A., 2005. Eigenvector-based spatial filtering for reduction of physiological interference in diffuse optical imaging. J. Biomed. Opt. 10, 011014.